# EGFR-targeted semiconducting polymer nanoparticles for photoacoustic imaging

Sciscione, Fabiola; Guillaumé, Simon; Aliev, Abil E.; Cook, Declan T.; Bronstein, Hugo; Hailes, Helen C.; Beard, Paul C; Kalber, Tammy L; Ogunlade, Olumide; Tabor, Alethea B.

*DOI:*
10.1016/j.bmc.2023.117412

Bioorg. Med. Chem. 91 (2023) 117412

Contents lists available at ScienceDirect

Bioorganic & Medicinal Chemistry

journal homepage: www.elsevier.com/locate/bmc

# EGFR-targeted semiconducting polymer nanoparticles for photoacoustic imaging

Fabiola Sciscione [a], Simon Guillaumé [a], Abil E. Aliev [a], Declan T. Cook [a], Hugo Bronstein [b], Helen C. Hailes [a], Paul C. Beard [c], Tammy L. Kalber [d], Olumide Ogunlade [c,1], Alethea B. Tabor [a,*]

[a] Department of Chemistry, University College London, 20, Gordon Street, London WC1H 0AJ, UK
[b] Yusuf Hamied Department of Chemistry, University of Cambridge, Lensfield Road, Cambridge CB2 1EW, UK
[c] Department of Medical Physics and Biomedical Engineering, University College London, Malet Place Engineering Building, Gower Street, London WC1E 6BT, UK
[d] Centre for Advanced Biomedical Imaging, University College London, Paul O'Gorman Building, London WC1E 6DD, UK

A B S T R A C T

Semiconducting polymer nanoparticles (SPN), formulated from organic semiconducting polymers and lipids, show promise as exogenous contrast agents for photoacoustic imaging (PAI). To fully realise the potential of this class of nanoparticles for imaging and therapeutic applications, a broad range of active targeting strategies, where ligands specific to receptors on the target cells are displayed on the SPN surface, are urgently needed. In addition, effective strategies for quantifying the level of surface modification are also needed to support development of ligand-targeted SPN. In this paper, we have developed methods to prepare SPN bearing peptides targeted to Epidermal Growth Factor Receptors (EGFR), which are overexpressed at the surface of a wide variety of cancer cell types. In addition to fully characterising these targeted nanoparticles by standard methods (UV–visible, photoacoustic absorption, dynamic light scattering, zeta potential and SEM), we have developed a powerful new NMR method to determine the degree of conjugation and the number of targeting peptides attached to the SPN. Preliminary *in vitro* experiments with the colorectal cancer cell line LIM1215 indicated that the EGFR-targeting peptide conjugated SPN were either ineffective in delivering the SPN to the cells, or that the targeting peptide itself destabilised the formulation. This in reinforces the need for effective characterisation techniques to measure the surface accessibility of targeting ligands attached to nanoparticles.

## 1. Introduction

Photoacoustic imaging (PAI) is a relatively new imaging modality that has great potential for imaging the cellular and molecular biomarkers of cancer.[1] PAI can provide molecular imaging in real-time at exceptionally high resolution, from ~1 μm at a penetration depth of around 1 mm, to >250 μm at depths of several cm. In contrast to many other cancer imaging modalities, such as PET and MRI, PAI does not involve the exposure of patients to ionising radiation and does not require complex and costly scanners. Moreover, endogenous biological chromophores, such as water, melanin and haemoglobin, absorb strongly in the visible region.[1,2] For all of these reasons, PAI is an excellent modality for imaging the vasculature, for the detection and monitoring of breast, lung, head and neck cancers and melanomas, and for biopsy and surgery guidance.[3]

However, at visible and UV wavelengths strong tissue scattering attenuates the PA signal, making deep tissue imaging difficult. In addition, many therapeutically relevant biological markers are optically silent. A wide variety of exogenous PA contrast agents are therefore currently being developed. Contrast agents for PA imaging should have high molecular extinction coefficients, excellent photostability, low toxicity, an adequate *in vivo* lifetime and low immunogenicity as well as high target affinity and specificity. In addition, since PAI relies on the conversion of light to heat, fluorescent probes with high quantum yields are precluded from use. In both the NIR-I (650–900 nm)[2] and NIR-II (1000–1400 nm)[4] regions tissue scattering is low, and chromophores absorbing in these regions are currently being exploited for deep tissue PAI. Chromophores absorbing in the NIR-I region are of particular interest; this range is known as the optical window of tissue due to the low absorption of water and haemoglobin at these wavelengths.[2]

A variety of new, non-fluorescent PA contrast agents are being developed, such as single-walled carbon nanotubes (SWCNT) and gold nanoparticles (AuNP).[2,5] However, many of these have only moderate molar extinction coefficients, as well as poor photostability, a tendency to aggregate and poor toxicity/biodegradability. Alongside their applications in molecular electronics and photovoltaics, semiconducting

* Corresponding author.
*E-mail address:* a.b.tabor@ucl.ac.uk (A.B. Tabor).
[1] Present address: Institute of Cardiovascular Sciences/School of Engineering, University of Birmingham, UK.

https://doi.org/10.1016/j.bmc.2023.117412
Received 7 April 2023; Received in revised form 7 July 2023; Accepted 10 July 2023
Available online 11 July 2023

polymers (SP) have in the last decade attracted attention for use in PAI.[6–9] Their extensive, highly delocalised π-conjugated backbones give SP a narrow band gap, facilitating photoexcitation and energy transfer and conferring excellent opto-electronic properties. Their organic composition also carries less potential for toxic degradation than their inorganic counterparts. The inherent hydrophobicity of SP allows them to be formulated into nanoparticles alongside oligomers and lipids, to form semiconducting polymer nanoparticles (SPN). These have large absorption coefficients, controllable sizes, adjustable absorption maxima, optical properties that are independent of particle size, and high photostability. The majority of reported SPN have been formed through the co-precipitation of lipids and SP, via either nano-precipitation[10] or mini-emulsion.[11] These techniques effectively encapsulate a water-insoluble, conjugated polymer within a water-soluble, liposome-like construct. Amphiphilic SP can also undergo crystallisation-driven self-assembly in solution to form nanoparticles with a core–shell architecture,[12] and more recently microfluidic processing systems have been shown to enable large scale, high throughput production of uniform SPN.[13,14] Over the last decade, different SPN have been developed with a range of SP, liposomal formulations and PEGylation approaches, leading to nanoparticles with long *in vivo* lifetimes, good biodistribution profiles and maximum absorbance tuned to the NIR-I or NIR-II regions.[7,15,16] SPN were first described for *in vivo* PAI in 2014;[17] the SP used in this study, poly(cyclopentadithiophene-*alt*-benzothiadiazole) (PCPDTBT) and poly(acenaphthothienopyrazine-*alt*-benzodithiophene), had absorption maxima at around 660 and 700 nm, respectively, giving SPN with better photostability and higher PA intensity in the NIR region than SWCNTs and AuNP. Pu *et al.* recently demonstrated the synthesis and metabolic pathway of a SPN designed to absorb in the NIR-II window.[18] Poly benzobisthiadiazole (PBBT) SP, selected for their strong absorption in the second NIR window of absorption, were co-formulated with FDA approved, biodegradable and amphiphilic PLGA-PEG oligomers by nanoprecipitation. The resulting SPN had excellent PAI properties, and the metabolic byproducts were also shown to be effectively cleared from live animals via both hepatobiliary and renal clearance. We have recently described a series of SPN with tunable absorption properties in the NIR-I window, using indigoid π-conjugated SP with a high extinction coefficient and a narrow band-gap.[19].

These recently developed highly sensitive exogenous PA contrast agents, in parallel with advances in instrumentation, are bringing PAI closer to clinical use for cancer screening, imaging of primary tumours and metastases, and image-guided surgery.[1] One of the remaining challenges limiting the clinical use of PAI is limited imaging contrast, and this can be partly overcome by using precisely targeted exogenous contrast agents which can be tuned to different NIR-I or NIR-II frequencies. In particular, for PAI to be an effective means of imaging and treating cancer, exogenous contrast agents must selectively localise at the tumour. Passive uptake and accumulation of nanoparticles in tumour tissue occurs via the Enhanced Permeability and Retention (EPR) effect. The defective vasculature surrounding tumours leads to a greater macromolecular leakage from the blood vessels into the interstitial tumour space, and the lack of lymphatic drainage from tumour tissues leads to the accumulation of macromolecules of sizes 50–200 nm in those sites.[20] The EPR effect has been one of the major driving forces behind the development of many nanomedicines including drug encapsulating polymer conjugates, liposomes, and micelles. Nanomedicines with sizes between 100 and 200 nm have shown improved pharmacokinetics and preferential tumour uptake in animal models. Unfortunately, the majority of these nanomedicines have then shown little or no efficacity in human clinical trials, which has led to a revision of the viability of the EPR effect alone to direct nanoparticle treatments to tumours.[21,22] Several approaches have been proposed to complement the EPR-mediated delivery of nanotherapeutics, in particular "active targeting" strategies where a targeting ligand is displayed on the nanoparticle surface. These are particularly beneficial as they are synthetically accessible, can be easily modified to give individualised treatments tailored to patient tumour type, and can draw on a range of different techniques developed for bioconjugation.[23] So far, the majority of SPN reported for PAI have relied on passive accumulation of the nanoparticles at the tumour site.[24] Recently, SPN have been adapted for active targeting of tumours by modification of the surface with cRGD peptides,[25] prostate-specific membrane antigen targeting ligands,[26] folic acid[27] and by coating the SPN with activated fibroblast (AF) cell membranes.[28] Thrombus-targeting SPN have also been developed by surface modification with cRGD peptides.[29] However, there is a need to develop a broader repertoire of surface modifications of SPN to allow a wide range of modalities of active targeting to different cancer cell types, and to understand how to optimise bioconjugation methods, peptide sequence and linker structure to give effective surface modification and receptor availability.

In this study, we have focussed on SPN bearing peptides targeted to Epidermal Growth Factor Receptor (EGFR), a cell-surface receptor belonging to the ErbB family of tyrosine kinases.[30] Overexpression and dysregulation of EGFR occurs in a wide variety of cancer types, and EGFR is a validated target for molecular cancer therapeutics.[31] Extensive research has been carried out in the last 20 years on the development of monoclonal antibodies, antibody fragments and peptide sequences which target EGFR.[32,33] The peptide sequence GE11 (YHWYGYTPQNVI)[34,35] was identified via phage-display screening, D4 (LARLLT)[36] was identified from screening a peptide library *in silico* against the X-ray crystal structure of EGFR, and A-R (AEYLR)[37] was derived from the native autophosphorylation site of EGFR. These have all been used successfully as active targeting agents for antitumour therapy. We have previously developed lipopolyplexes with EGFR-targeting peptides at the surface as theragnostic vectors for non-viral gene delivery, and have demonstrated that these selectively and efficiently transfect tumour cells with pDNA coding for optical imaging (firefly luciferase, green fluorescent protein)[38] or for a biosensor for FRET-FLIM imaging[39,40] *in vitro* and *in vivo*. We have demonstrated that for different cancer cell types, nanoparticle formulations and surface bioconjugation methods, it is necessary to evaluate each of these peptide sequences. Subtle differences in both target cell receptor structure and steric availability of the targeting sequence determine the optimal targeting sequence for binding to the surface, and/or internalisation, for different cell types.[38,39,40] In this study, we have formulated and characterised SPN PAI agents that have been functionalised via bioconjugation of all three of these EGFR-targeting peptides. These SPN have low polydispersity and excellent PA properties. We have characterised the degree of surface coverage of the peptides using a novel NMR approach and have evaluated the availability of the peptide ligands for targeted uptake to colorectal cancer cells.

## 2. Materials and methods

### 2.1. Chemicals

1,2 Dipalmitoyl-*sn*-glycerol-3-phosphocoline (DPPC), 1,2-distearoyl-*sn-glycero*-3-phosphoethanolamine-*N*-[maleimide(polyethylene glycol)-2000] (ammonium salt) (DSPE-$PEG_{2000}$-malemide) and 1,2-distearoyl-*sn-glycero*-3-phosphoethanolamine-*N*-[amino(polyethylene glycol)-2000] (ammonium salt) (DSPE-$PEG_{2000}$-Amine) were purchased from Avanti Lipids, USA. Poly-[cyclopentadithiophene-*alt*-benzothiadiazole] (PCPDTBT; $M_W = 7000–20000$ kDa) was purchased from Sigma-Aldrich.

**Table 1**
SPNs formulations with different total lipid concentrations and molar ratios.

| | SPN I | SPN II | SPN III | SPN IV |
|---|---|---|---|---|
| DPPC (mol %) | 95 | 90 | 95 | 90 |
| DSPE-$PEG_{2000}$-malemide (mol %) | 5 | 10 | 5 | 10 |
| Total lipid concentration (mg/ml) | 0.25 | 0.25 | 2.5 | 2.5 |
| PCPDTBT (mg/ml) | 0.25 | 0.25 | 0.25 | 0.25 |

All other chemicals were obtained from Sigma-Aldrich unless otherwise stated. All peptide sequences (Table 1) were synthesised via solid-phase peptide synthesis. Peptides **Cys-AR**, **Cys-GE11** and **Cys-D4** were synthesised as previously reported.[38] The synthetic procedure, purification methods and characterisation for **Cys-EEG-GE11** is included in the Supporting Information.

### 2.2. SPN synthesis

SPN were prepared via a nanoprecipitation method using our previously reported protocol.[19] Briefly, 1 mL of PCPDTBT in THF at a concentration of 0.25 g/L was quickly injected with a syringe into 9 mL of Milli-Q water under constant sonication using an ultrasonic tip (QSonic probe; Q125) for 30 s in an ice bath (6 W RMS). 1 mL of a lipid mixture of DPPC/DSPE-$PEG_{2000}$-malemide prepared in THF/water (2:3 v/v) was added to the aqueous dispersion and this was further sonicated for 60 s at 6 W RMS. The total lipid concentration and the molar ratios used for each of the formulations are shown in Table 2. The THF was then evaporated by stirring the above mixture at 45 °C in a water bath for 3 h under nitrogen flow. The resulting SPN were filtered through a 0.22 mm poly-ethylene-sulfone syringe-driven filter (Merck Millipore, US) and purified with Amicon® centrifuge filters (Ultra-4-Centrifugal Filter Unit [MWCO 30 kDa], Merck Millipore, US) at 2780 *g* for 5 min at 4 °C. This was repeated three times and each time the pellet was resuspended in 2 mL of Milli-Q water. The SPN suspension was stored at 4 °C at a final volume of 2 mL in MilliQ-water.

The SPN used as a negative control for *in vitro* work were prepared as described above using DPPC/DSPE-$PEG_{2000}$-Amine as the lipid mixture.

The SPN used for NMR studies were prepared as described above using $D_2O$ as a solvent. In the last centrifugation step the pellet was resuspended to a final volume of 500 mL in $D_2O$ prior to NMR measurements.

### 2.3. Conjugation of EGFR-targeting peptides to SPN

A solution of the EGFR-targeting peptide (10 mg/mL) was prepared in 0.1 M phosphate buffer at pH = 7.4 containing 5 mM of TCEP. Freshly prepared SPN suspension in MilliQ-water (2 mL) were concentrated with Amicon® centrifuge filters (Ultra-4-Centrifugal Filter Unit [MWCO 30 kDa], Merck Millipore, US) at 2780 *g*RCF at 4 °C until a volume of 50–100 μL was reached and this was then diluted to a final volume of 1 mL in phosphate buffer. Subsequently, 15 eq. of EGFR targeting peptide in phosphate buffer were added to the SPN solution and the mixture was left under agitation for 4 h at room temperature. The reaction was monitored by $^1$H NMR, with the complete disappearance of maleimide $^1$H proton shifts (Fig. 4b) indicating complete conjugation. Upon completion of the reaction, the mixture was diluted to 2 mL using Milli-Q water, washed three times by centrifugation (2780 *g* RCF 5 mins at 4 °C) to remove unreacted peptide, and concentrated to a final volume of 150 μL. The filtrates from the centrifugation washes were analysed for the presence of residual, unreacted peptide. The analysis of the washing filtrates by UV spectroscopy at 280 nm showed no residual peptide absorption after the third round of centrifugation.

The EGFR-targeting peptide conjugated-SPN used for NMR studies were obtained from freshly prepared SPN suspension in $D_2O$ and using 0.1 M deuterated phosphate buffer (pD = 7.4) for the conjugation reaction with EGFR-targeting peptides.

**Table 2**
Hydrodynamic diameter ($D_H$) and ζ-potential values for SPN I, II, III and IV in Milli-Q $H_2O$. Measurements were carried out at room temperature.

| Formulation | $D_H$ (nm) | PdI | ζ (mV) |
|---|---|---|---|
| SPN I | 97.17 ± 1.85 | 0.197 ± 0.011 | −43.73 ± 0.86 |
| SPN II | 96.28 ± 1.19 | 0.197 ± 0.007 | −45.61 ± 0.35 |
| SPN III | 97.10 ± 0.65 | 0.241 ± 0.001 | −46.52 ± 0.53 |
| SPN IV | 99.67 ± 0.42 | 0.203 ± 0.007 | −40.84 ± 1.29 |

### 2.4. Nuclear magnetic resonance (NMR)

NMR ($^1$H and $^{13}$C, DEPT, NOESY, COSY, HMQC, HMBC) was performed on a 700 MHz Avance Neo Bruker spectrometer equipped with a 5 mm broadband cryoprobe. The chemical shifts (δ) are given in units of ppm relative to tetramethylsilane (TMS), where δ (TMS) = 0 ppm. Coupling constants (J) are measured in Hertz (Hz), multiplicities for $^1$H coupling are shown as s (singlet), d (doublet), t (triplet), m (multiplet), or a combination of the above. Deuterated water ($D_2O$) was used as solvents (as stated) for all NMR measurements.

### 2.5. Assessment of maleimide functionality on the surface of SPNs and peptide conjugation by NMR

A single pulse experiment was used to measure $^1$H NMR spectra. A 30° pulse was used. In order to exclude relaxation time effects, the acquisition time was set to 4 s and the relaxation delay was set to 36 s. Thus, the repetition time was 40 s, allowing full relaxation prior to the application of each pulse. 32 scans were acquired for each run. The $^1$H NMR spectra of the SPNs in $D_2O$ were compared to that of DSPE-PEG2000-maleimide in $D_2O$ for the qualitative assessment of the presence of maleimide moieties on the SPNs. Quantitative assessment was performed in $D_2O$ by using maleic acid as internal standard at a concentration of 0.1 mM. Concentration of maleimide groups ($C_{\text{maleimide groups}}$) in the nanoparticle suspension was calculated according to Equation (1), where $C_{IS}$ is the concentration of the internal standard, $I_{\text{maleimide groups}}$ is the integral relative to the maleimide groups present in the nanoparticle suspension, #maleimide protons is the number of maleimide protons, $I_{IS}$ is the integral value of the internal standard and #IS protons is the number of internal standard protons:

$$C_{maleimide\ groups} = C_{IS}\left(\frac{I_{maleimide\ groups}/\#maleimide\ protons}{I_{IS}/\#\ IS\ protons}\right) \quad (1)$$

**Equation (1):** Calculation of the concentration of maleimide groups in the nanoparticle dispersion by $^1$H NMR in $D_2O$.

Similarly, the $^1$H NMR spectrum of Cys-A-R in $D_2O$ was used to quantitively assess the presence of the peptide on the surface of the SPNs by following the appearance of the aromatic protons of the tyrosine residue and using maleic acid as the internal standard at a concentration of 0.1 mM. The concentration of tyrosine groups was calculated in a similar way to the calculation of maleimide groups in Equation (1).

### 2.6. Scanning electron microscopy

Scanning Electron Microscopy (SEM) was performed using a Carl Zeiss XB1540 Crossbeam SEM/FIB at the London Centre for Nanotechnology (LCN). A drop of the sample (diluted by 10-fold in Milli-Q water) was placed onto a silicon wafer and left to dry overnight. Subsequently, the sample was gold-sputtered before imaging (Edward Sputter Coater). The diameter of the nanoparticle was measured with ImageJ. Statistical analysis on the frequency count was done with Origin Pro 9.1 and these data were fitted with a LogNormal distribution using the same software.

### 2.7. Dynamic light scattering and ζ potential measurements

The hydrodynamic diameter ($D_H$) and z-potential of SPNs and EGFR-targeting peptide-conjugated SPNs were measured with a Zeta-sizer Nano (Malvern Instrument Ltd., UK). Nanoparticle samples were diluted by 10-fold in an appropriate solvent medium and filtered through a 0.45 mm PES syringe-driven filter before the measurement. The hydrodynamic diameter and ζ-potential were measured in ultrapure Milli-Q water. The software uses the CONTIN analysis to obtain the intensity distribution and the cumulant analysis to generate the

hydrodynamic diameter and polydispersity index values. All measurements were performed in triplicate.

### 2.8. UV–visible spectroscopy (UV–vis)

UV–vis spectroscopy was carried out on an Agilent Cary 100 UV–Vis spectrophotometer, using a 0.5 mL quartz cuvette with a 10 mm path length. Spectra were acquired from 300 to 1000 nm in ultrapure Milli-Q water for the nanoparticle samples and in THF for PCPDTBT.

### 2.9. PA spectroscopy

PA absorption spectroscopy was carried out on a custom-built PA spectroscope.[19] The absorption coefficient was determined by fitting an exponential to the initial compressive part of PA signals generated by 1 mg/mL SPN solutions contained in a cuvette. The volume of the solutions was 50 μL.

### 2.10. Cell uptake studies

The human LM1215 colorectal carcinoma cell line, positive for EGFR expression[39,40] was grown in RPMI-1640 (Life Technologies Ltd) supplemented with 10 % fetal calf serum (FCS, Invitrogen, Paisley, UK), in a humidified incubator at 37 °C with 95 % air and 5 % $CO_2$. Cells were grown to 80 % confluence before trypsinisation and centrifugation for pelleting at 300g. The cells were counted and then plated overnight at $1x10^6$ in 6 well plates for in vitro uptake studies. The growth media was removed, the cells washed with PBS and 2 mL of serum free RPMI-1640 media was added. Prior to cell uptake work freshly prepared SPN in MilliQ-water (2 mL) was concentrated with Amicon® centrifuge filters (Ultra-4-Centrifugal Filter Unit [MWCO 30 kDa], Merck Millipore, US) at 2780 *g* RCF at 4 °C until a volume of 500 mL was reached. 250 μL of SPN III formulations (Table 3) were added in duplicate to the wells and 250 μL of sterile water was added in duplicate to control no-SPN wells and the cells were incubated for 4 h in the incubator at 37 °C. After incubation the cells were washed 3 times with PBS before trypsinisation and centrifugation for pelleting at 300g for the assessment of successful uptake by green colouration of the pellet.

## 3. Results

### 3.1. Targeted SPN formulation and bioconjugation strategy

Surface functionalisation of liposomes for active targeting is generally achieved either by bioconjugation of the targeting peptide to activated groups at the surface of liposomes, or by synthesis of a suitable lipid-targeting peptide bioconjugate, followed by liposome formulation.[41] Whilst prior synthesis of a lipid-targeting peptide bioconjugate has the advantage that the bioconjugate can be fully characterised prior to formulation, purification of such lipopeptides is frequently challenging and the presence of the targeting peptide can impede formulation of the SPN. We therefore elected to use the commercially available DSPE-$PEG_{2000}$-maleimide as the activated lipid, formulated at varying concentrations with DPPC, with the aim of subsequently developing a reliable analytical method for characterising the extent of post-formulation bioconjugation to give targeted SPNs (Fig. 1A). To enable thiol-maleimide Michael addition[42] between the targeting peptide and the maleimide displayed at the SPN surface, we synthesised the AR, GE-11 and D4 peptide sequences with Cys residues at the *N*-terminus, giving peptides **Cys-AR**, **Cys-GE-11** and **Cys-D4**, respectively. For the π-conjugated organic semiconducting polymer component, we used the commercially available PCPDTBT. This SP has a broad absorption spectrum in the NIR-I window, a high molar extinction coefficient and low fluorescence conversion. SPN formulated from PCPDTBT have excellent properties for *in vivo* PAI, with significantly better PA signal and photostability than high performing gold nanorods or SWNT.[17,43,44].

In our previous work,[19] we had used both nanoprecipitation and mini-emulsion techniques to prepare the SPN, depending on the solubility characteristics of the SP. The mini-emulsion approach is generally used when a hydrophobic polymer does not dissolve in any water-miscible solvents. The emulsion is formed by adding a semiconducting polymer dissolved in organic solvent to a water solution containing dispersed or dissolved surfactants: evaporation of the organic solvent results in a stable solution of SPN.[45] In contrast, nanoprecipitation methods are primarily used when the conjugated polymer has good solubility in a water-miscible, organic solvent. Once dissolved in such a solvent, the resulting polymer solution is rapidly injected into a large excess of water under sonication. The formation of nanoparticles is driven by the change in polarity of the solvent mixture, which results in aggregation of the conjugated polymers in solution. Removal of the organic phase yields spherical SPN, whose size depends on the concentration of polymer during the formation process.[46,47] As PCPDTBT has good solubility in THF, we elected to use nanoprecipitation in water and THF for the preparation of the SPNs. An overview of the nanoprecipitation method used is shown in Fig. 1C. Four SPN formulations (SPN I, SPN II, SPN III, SPN IV) with a total lipid concentration of either 0.25 or 2.50 mg/mL and two different molar ratios of DSPE-$PEG_{2000}$-maleimide, either 95:5 or 90:10 mol % were investigated (Table 1).

The average hydrodynamic diameter ($D_H$) and the zeta potential (ζ) of the SPNs were measured by dynamic light scattering and electrophoretic mobility respectively. The values are reported in Table 2 below. The intensity distribution showed a fairly monodisperse population for all SPNs (Fig. SI 1 a). The $D_H$ and ζ-potential were not significantly affected by the different lipid concentrations and/or molar ratios investigated (Table 2, Fig. S1a and S1b). The formulations were stored at 4 °C and were stable over a 6-week period in Milli-Q $H_2O$ (Fig. S2).

The normalised UV–visible spectra of the SPNs in Milli-Q $H_2O$ and of PCPDTBT in THF are shown in Fig. 2a below. A slight hypsochromic shift of the absorption maximum at 705 nm was observed for all SPNs compared to that of PCPDTBT, with SPNI and SPN II showing the largest shift respect to SPN III and SPN IV. Overall, all formulations retained PCPDTBT optical properties in the NIR region of the spectrum. None of the SPN formulations showed any detectable fluorescence, indicating that radiative decays are not the main energy loss mechanisms, as already observed in our previous work.[19]

The PA properties of the aqueous solutions of all SPNs were measured by a custom-made PA spectroscope and the resulting extinction spectra are reported in Fig. 2b. SPN III showed the highest PA signal and was chosen as the SPN formulation used for the subsequent conjugation with the EGFR-targeting peptides.

**Table 3**
$I_{maleimide\ group}$ values and the respective concentrations of the maleimide group for three measurements calculated from Equation (1).

| Measurement | $I_{maleimide\ group}$ (6.91 ppm) | $I_{IS}$ (6.33 ppm) | Concentration of maleimide groups ($10^{-4}$ M)[1] |
|---|---|---|---|
| 1 | 2.070 | 1.00 | 2.07 |
| 2 | 2.123 | 1.00 | 2.12 |
| 3 | 2.031 | 1.00 | 2.03 |
| Yield ( %) | | | 69.12 ± 1.54 |

[1] Theoretical concentration of maleimide groups is $3.0 \times 10^{-4}$ M.

### 3.2. Conjugation of EGFR targeting peptides to SPN III and characterisation of SPN III-Cys-AR

In order to determine the level of modification by EGFR targeting peptides, the presence of maleimide moieties incorporated in the SPN III formulation was first confirmed by $^1$H NMR. In the SPN III spectrum the two maleimide protons appear as a singlet at 6.91 ppm (Fig. 3) away from the upfield region of the spectrum (<6 ppm) crowded by the

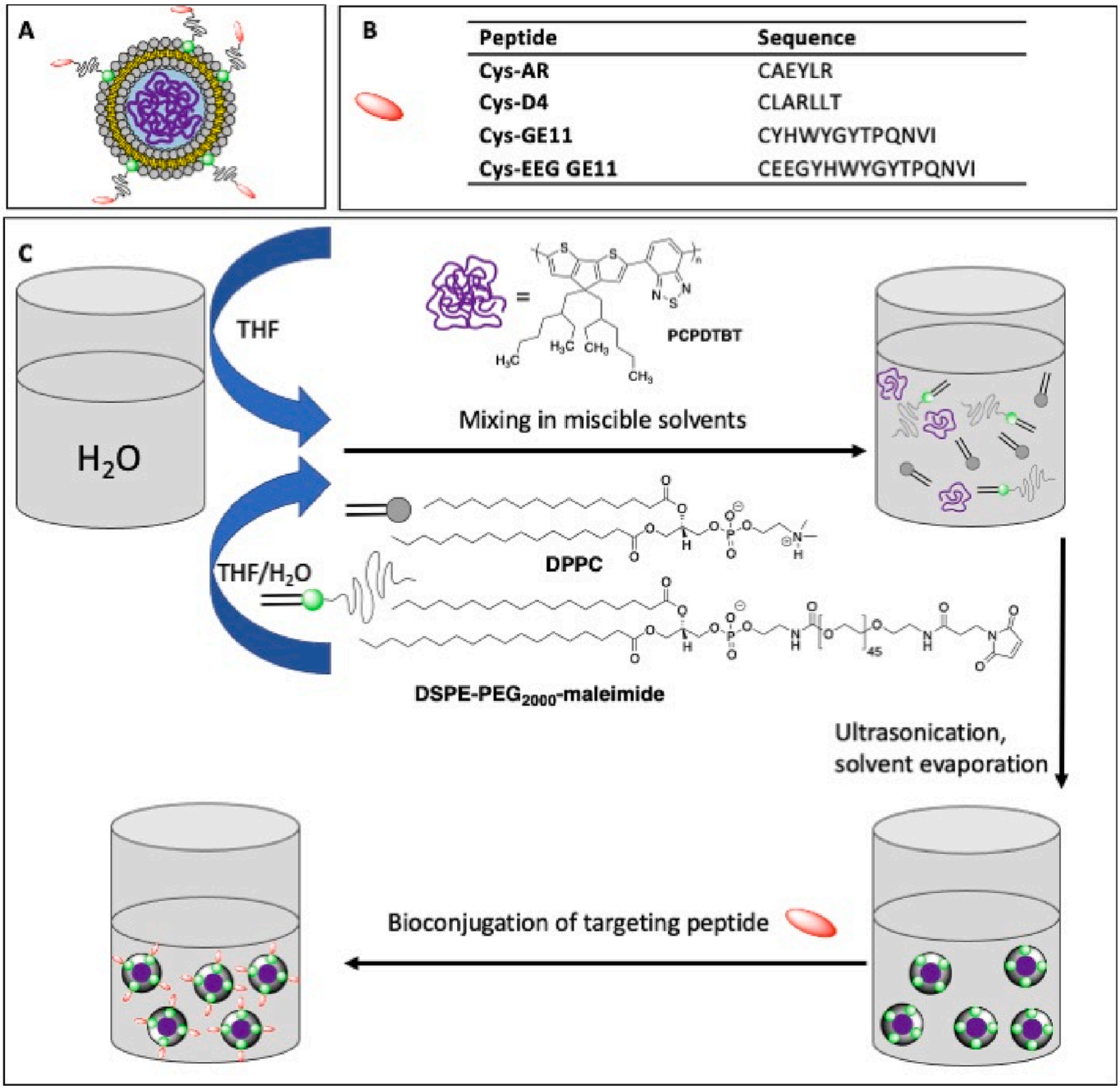


**Fig. 1.** (A) General schematic of the SPN, (B) sequences of EGFR targeting peptides used in this study. (C) Schematic representation of the nanoprecipitation method used to prepare the SPN.

presence of PEG and other lipid components (See Fig. S3 for the full spectrum). The signal for the maleimide protons in isolated DSPE-$PEG_{2000}$-malemide has been previously reported to occur at 6.92 ppm.[48] The amount of maleimide functional groups in the SPN III suspension was quantified by $^1$H NMR in $D_2O$ using maleic acid as the internal standard at a concentration of 0.1 mM (signal at 6.33 ppm in Fig. 3). Maleic acid was chosen for its solubility in water as well as the convenient location of its proton shifts in a region where there is no overlap with other signals from SPN III (>6 ppm). The concentration of maleimides in the suspension was calculated according to Equation (1) (see Methods) by comparing the integral intensity values of the signal at 6.91 ppm ($I_{\text{malemide group}}$ ) relative to the maleimide groups present on the nanoparticle surface to the integral intensity value of the internal standard ($I_{IS}$) at 6.33 ppm which was normalised to one. The $I_{\text{malemide group}}$ values and the respective calculated concentrations for three measurements are reported in Table 3. The calculated yield percentage of maleimide groups in the SPN III formulation was ca. 69 %. This in turn indicates that each nanoparticle has around 6000 maleimide groups that can be detected, although not all of these will be at the surface of the SPN.

Having successfully characterised the level of maleimide modification of the SPN III formulations by $^1$H NMR, EGFR targeting peptides (Fig. 1b) were then conjugated to the surface of SPN III via thiol-maleimide Michael addition in phosphate buffer (Scheme 1).

The presence of the Tyr residue in the A-R sequence offered a good opportunity to monitor and characterize the conjugation of Cys-AR to the surface of SPN III, by following the appearance of the aromatic proton signals of the Tyr side chain. In the $^1$H NMR spectrum of

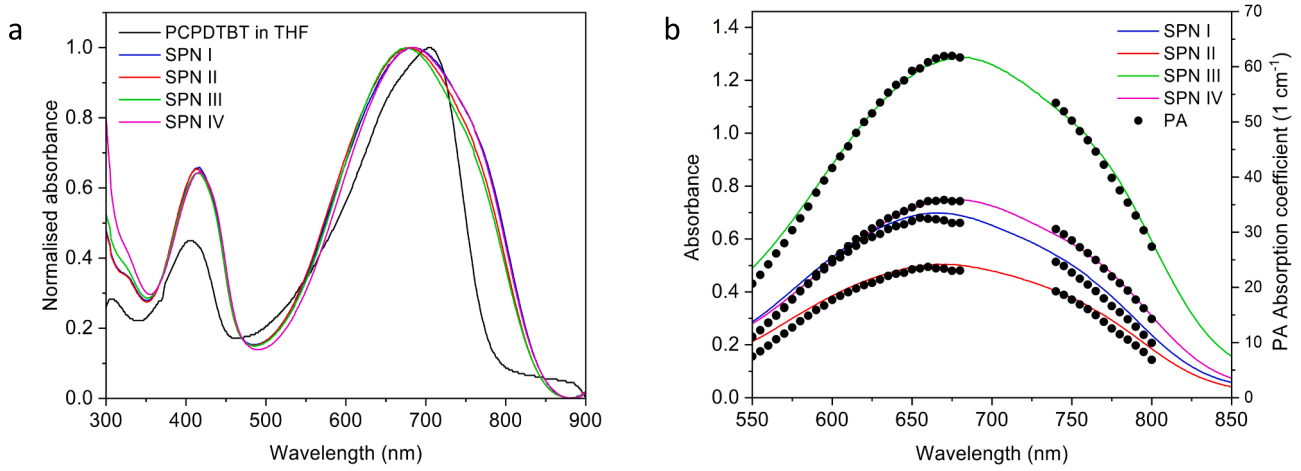


**Fig. 2.** (a) Normalised UV–visible spectra of SPN I–IV and PCPDTBT; (b) Absorbance spectra of SPN I–IV (solid line), PA derived absorption coefficient spectra of SPN I–IV (dotted lines).

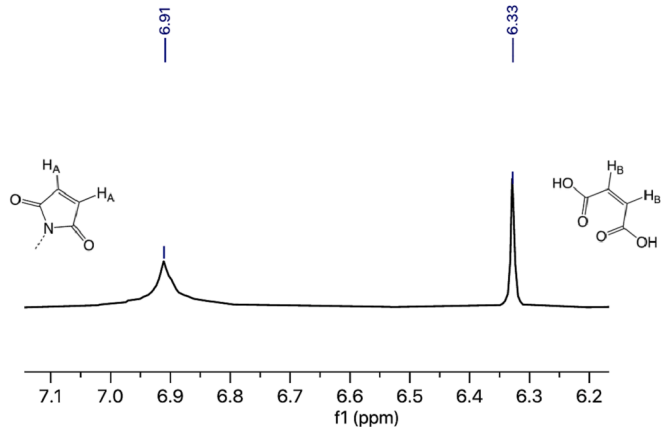


**Fig. 3.** $^{1}$H NMR spectra in $D_2O$ of SPN III, showing the maleimide protons at 6.91 ppm and maleic acid used as the internal standard protons at 6.33 ppm. The full spectrum is shown in Fig. S3 in the Supporting Information.

unconjugated Cys-AR in $D_2O$, these signals appear as two doublets found at $\delta = 7.08$ ppm and $\delta = 6.77$ ppm (Fig. 4a). Upon conjugation, the appearance of the aromatic proton signals of the tyrosine residue and complete disappearance of maleimide $^{1}$H proton shifts were observed (Fig. 4b) indicating complete conjugation. The formation of the succinimide-thiol adduct could not be directly observed, since upon thiol addition, the resulting succinimide protons are shifted upfield (2.5–4.5 ppm), in a region dense with proton signals from the peptide and lipid-PEG conjugates also present in the $^{1}$H NMR spectra of SPN III. A change of the chemical shift was observed for maleic acid. This change from 6.33 ppm (Fig. 3) to 6.01 ppm (Fig. 4b) is attributed to maleic acid being a protolyte. It has previously been demonstrated that when mixed with other protolytes, the chemical shift of the signal may change to some extent.[49] On increasing the concentration of maleic acid, the signal at 6.01 ppm shifts back to the usual value of 6.33 ppm (Fig. S5, Supporting Information) suggesting that no chemical transformation of maleic acid has occurred and the low frequency shift in Fig. 4b is caused by non-covalent interactions of maleic acid with Cys-AR SPN III, most likely with the Cys-AR fragment, as no chemical shift change was observed for the mixture of maleic acid with **SPN III** (Fig. 3)**.** Using Equation (1), the concentrations of the Tyr group and the yield percentage of Tyr groups in **Cys-AR SPN III** were calculated (Table 4), indicating that each SPN has about 7,800 targeting peptides.

The size and ζ-potential of **Cys-AR SPN III** was confirmed by DLS and electrophoretic mobility. The peptide conjugated SPN III showed larger sized nanoparticles (129.90 ± 0.85 nm) and a more negative charge (-51.09 ± 0.85) compared to the unconjugated SPN III (Fig. 5a and b). The **Cys-AR SPN III** formulation showed a fairly monodisperse distribution and proved to be stable over time (Fig. S6). SEM analysis showed the presence of spherical nanoparticles for both **SPN III** and **Cys-AR SPN III** (Fig. 5 c and d). Statistical analysis of the SEM images confirmed the results obtained from DLS in terms of size (Fig. e and f) with a mean diameter centred around 60 nm for **SPN III** and 78 nm for **Cys-AR SPN III**. The optical properties of PCPDTBT were not affected by the peptide conjugation as confirmed by UV–visible spectroscopy (Fig. S7).

Using the same methodology, thiol-maleimide conjugation of peptides **Cys-D4** and **Cys-GE11** to the core maleimide-functionalised **SPN III** was then carried out (Table 5) and their uptake to LIM1215 cells assessed.

### 3.3. *In vitro cell uptake*

SPN cell uptake was assessed in the EGFR positive human colorectal carcinoma cell line LIM1215. Incubation of SPNs over the 4-hour time period did not show any differences to cell adhesion (cell rounding or floating) indicative of cell cytotoxicity compared to control. As a positive control, uptake of the core maleimide-functionalised **SPN III** was first investigated. Visual inspection of the cell pellet showed that this formulation had a high uptake in LIM1215 cells (Fig. S8) at a level suitable for PAI. This apparently high level of uptake/cell adhesion most likely arises from the presence of the reactive maleimide groups at the surface of the SPN III, which will react with free thiol groups in cellular proteins and glycoproteins.[50] As a negative control, we prepared a non-targeted **SPN-amine** formulation using DPPC/DSPE-$PEG_{2000}$-Amine as the lipid mixture, and this did not show any uptake to the LIM1215 cells. Unfortunately, the **Cys-AR SPN III** and **Cys-D4 SPN III** also did not show any green colouration, indicative of uptake in this colorectal cell line compared to non-labelled controls (Fig. S9). As PAI is not sufficiently sensitive to detect signal where there is no visible uptake in the cell pellet, we did not scan these cells. The **Cys-GE11 SPN III** formulation appeared to show some uptake to the LIM1215 cell line. However, these nanoparticles were unstable at room temperature. Extensive precipitation and aggregation were observed after washing but prior to trypsinisation, which could not be distinguished from cell uptake by visual

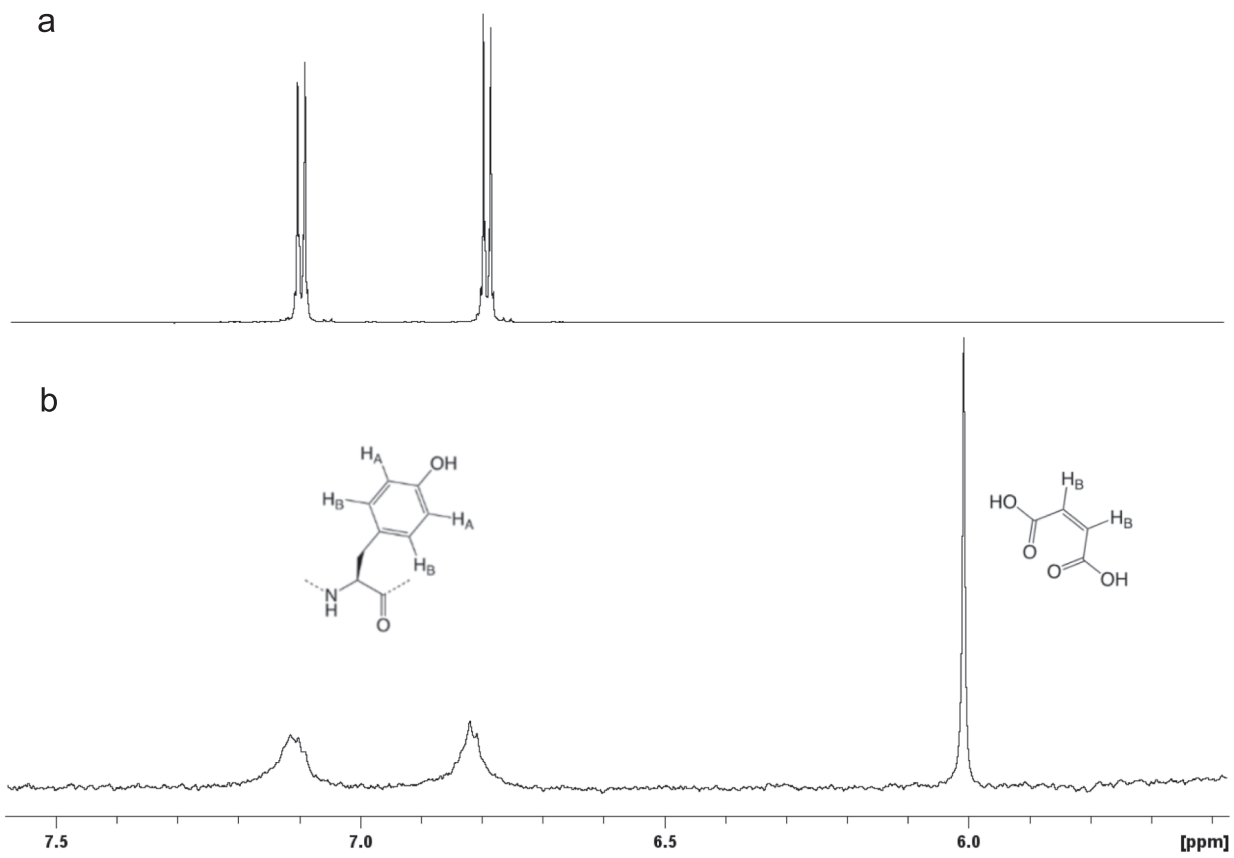


**Fig. 4.** (a)$^{1}$H NMR of Cys-A-R peptide in $D_2O$ (inset showing aromatic proton signals of the Tyr side chain); (b) $^{1}$H NMR of Cys-AR SPN III in $D_2O$ with 0.1 mM of maleic acid. Full spectra are shown in Fig. S4 in Supporting Information.

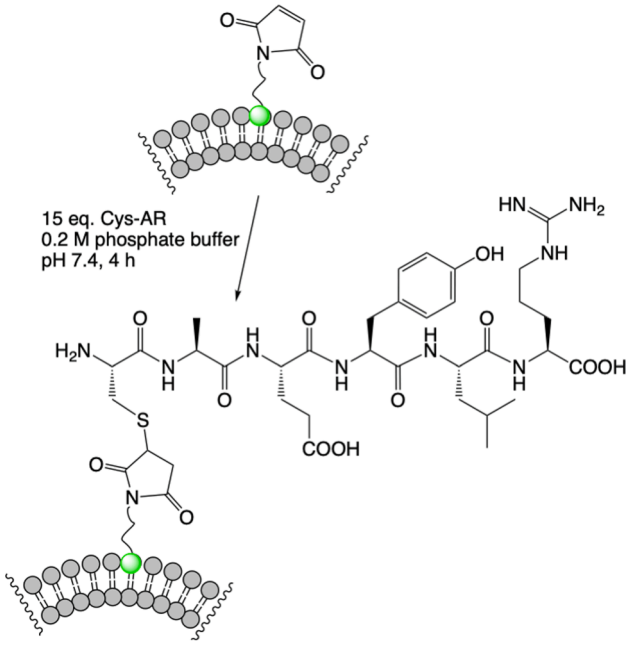


**Scheme 1.** Conjugation of Cys-A-R to SPN III via thiol-maleimide Michael addition.

**Table 4**
$I_{Tyr}$ values and the respective concentrations of the Tyr group for three measurements calculated from Equation (1).

| Measurement | $I_{Tyr}$ (7.11 & 6.82 ppm) | $I_{IS}$ (6.01 ppm) | Concentration of Tyr groups ($10^{-4}$ M)[1] |
|---|---|---|---|
| 1 | 2.257 | 1.00 | 1.13 |
| 2 | 2.092 | 1.00 | 1.46 |
| 3 | 2.264 | 1.00 | 1.11 |
| Yield ( %) | | | 59.38 ± 9.39 |

[1] Concentration of DSPE-$PEG_{2000}$-malemide from qNMR is $2.074 \times 10^{-4}$ M.

inspection when cells were pelleted. The more hydrophobic GE11 sequence is known to cause problems of aggregation when conjugated to nanoparticles and fluorophores.[51,52] We therefore synthesised **Cys-EEG-GE11**: the extra Glu residues in this sequence are known to improve the hydrophilicity of this peptide without altering the receptor targeting properties. This peptide was then conjugated to SPN III, however the resulting **Cys-EEG GE11 SPN III** formulation was still unstable and aggregated in media during cell uptake experiments.

## 4. Discussion and conclusions

SPN are very promising contrast agents for PAI of tumours, due to their size, excellent optoelectronic properties and high photostability. We have shown in this paper and in our previous work[19] that these formulations can be tuned, by adjusting the lipid composition and the structure of the incorporated SP, to optimise the PA signal and desired

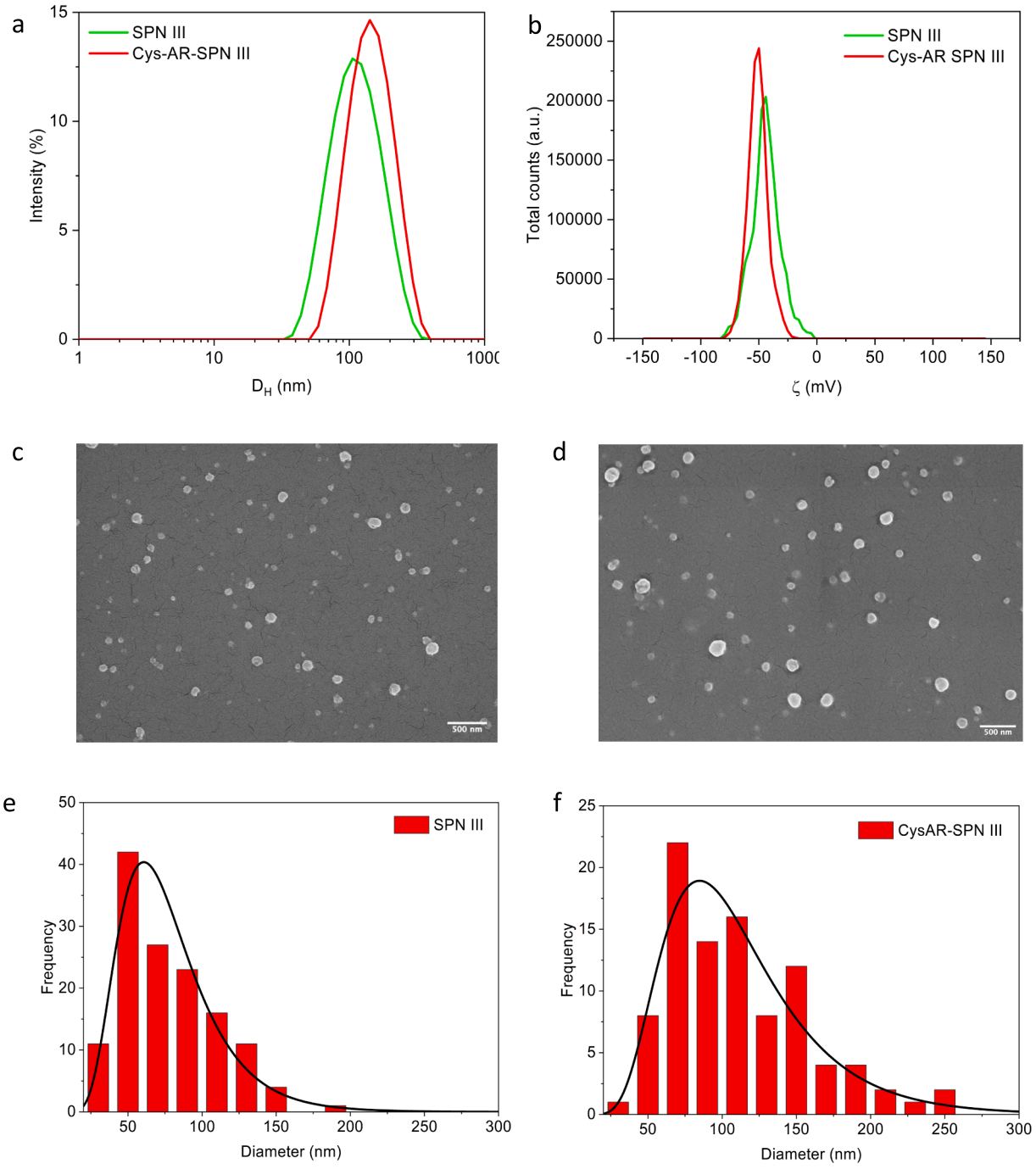


**Fig. 5.** (a) $d_H$ distribution and (b) ζ-potential of SPN III and Cys-AR SPN III; (c) SEM image of SPN III; (d) SEM image of Cys-AR SPN III; SEM statistical analysis of (e) SPN III and (f) Cys-AR SPN III, fitted with a LogNormal distribution (black curve).

**Table 5**
EGFR-conjugated SPN formulations.

| Formulation | Uptake to LIM1215 cells |
|---|---|
| SPN III | Yes |
| SPN-amine | Not detected |
| Cys-AR SPN III | Not detected |
| Cys-D4 SPN III | Not detected |
| Cys-GE11 SPN III | Formulation unstable |
| Cys-EEG GE11 SPN III | Formulation unstable |

wavelength. To achieve the goal of high-resolution accurate imaging of tumours, one of the remaining challenges is the selective delivery of SPN to tumour cells by bioconjugation of moieties such as peptides that will target receptors over-expressed at the surface of such tumour cells. Characterisation of the structural features of such peptide-targeted SPN is key to understanding and optimising their properties, and a reliable, rapid and non-perturbing method to quantitate the degree of peptide functionalisation is required. However, few methods for determining the efficiency of bioconjugation of peptides to the surfaces of nanoparticles have been reported. Where a chromophore can be added to the peptide

in question, fluorescence measurements or FRET assays can be used to quantitate the level of bioconjugation. This was recently reported for peptide-functionalised liposomal doxorubicin.[53].

Whilst quantitative NMR on nanoparticles has been previously reported, surprisingly, very few NMR studies have been carried out to characterise liposomes or other lipid-based nanoparticles.[54–56] To the best of our knowledge, this is the first time that quantitative NMR measurements have been applied for characterising the surface coverage of conjugated peptides. There are no reports of NMR methods for determining the level of peptide conjugation at the surface of liposomes, lipoplexes or SPN, although Epple and co-workers have recently successfully determined the level of peptide functionalisation at the surface of ultrasmall (2–5 nm) AuNP by $^{1}$H NMR,[57,58] suggesting that this might be a powerful method for assessing the coupling of peptide ligands to other types of nanoparticle.

In this paper, we have demonstrated that SPN can be formulated from mixtures of DPPC, DSPE-PEG$_{2000}$-malemide and the semiconducting polymer PCPDTBT to give nanoparticles that are uniform in size, have good PA properties and are stable over a two week period. We have bioconjugated these to peptides that have been extensively validated to bind to the EGFR and to target tumor cells for *in vitro* and *in vivo* cancer imaging and therapy. We have characterised these nanoparticles by DLS, electrophoretic mobility, SEM, UV–vis and PA, and have also developed a very powerful quantitative NMR (qNMR) method of analysis. This has enabled us to determine for the first time the concentration of maleimide groups in the initial SPN, and the number of peptides that are subsequently attached to each nanoparticle.

Disappointingly, these peptide-conjugated SPN showed little or no binding and uptake to a colorectal cell line known to overexpress these receptors. These three peptide sequences are known to vary in their binding affinity towards EGFR, uptake characteristics and affinity for different cancer cell types.[38–40,59] Indeed, in some cell lines the D4 peptide is completely ineffective for the selective delivery of small molecule drugs into EGFR-overexpressing cancer cells.[60] The more hydrophobic GE11 sequence is also not ideal, as it leads to tumor-targeted imaging agents with low solubility and a tendency to aggregation.[51,52] The lack of success of the peptide-targeted SPN reported in this work most likely reflects poor availability of the targeting ligands at the nanoparticle surface, combined with the destabilisation of the SPN when either Cys-GE11 or Cys-EEG-GE11 were attached.

In summary, this work demonstrates the importance of understanding the biophysical properties of different types of ligand-functionalised nanoparticles, particularly in view of the interest in lipid nanoparticles (LNP) as carriers for mRNA for vaccines, which became crucial during the COVID-19 pandemic.[61] In particular, for SPN imaging agents for targeted PAI, the effectiveness of the bioconjugation technique, the availability of targeting peptides at the surface of the nanoparticle and the stability of the resulting bioconjugate is crucial. This will require optimising the level of PEG coating and length of linker between the peptide and the nanoparticle,[62] and adjusting the interplay between the biophysical characteristics of the lipid, SP and peptide components. The new simple, accurate and rapid qNMR approach reported here will be vital for characterising the level of bioconjugation of ligands conjugated to a range of nanoparticles, and for subsequently developing the next generation of imaging agents.

## Declaration of Competing Interest

The authors declare that they have no known competing financial interests or personal relationships that could have appeared to influence the work reported in this paper.

## Data availability

Data will be made available on request.

## Acknowledgments

This work was supported by the CRUK City of London Centre Award [C7893/A26233] and [CTRQQR-2021/100004] (F. S.) We are also grateful for the financial support provided by the BBSRC LIDo PhD programme (BB/M009513/1: PhD studentship to S. G.), and for financial support from RC Grant 741149. O. O. was supported by a Research Fellowship from the UCL Wellcome/EPSRC Centre for Interventional and Surgical Sciences, and D. T. C. was supported by a PhD studentship funded by UCL Division of Biosciences. The EPSRC is also thanked for the equipment grant EP/P020410/1 *A 700 MHz broadband cryoprobe and NMR spectrometer at UCL Chemistry*.

## Appendix A. Supplementary material

Supplementary data to this article, including synthesis, purification and characterisation of **Cys-EEG-GE11**, $^{1}$H and biophysical data for **SPNIII** and **Cys-AR SPN111**, and preliminary cell uptake data, is available and can be found online at https://doi.org/10.1016/j.bmc.2023.117412.

## References

[1] Sternberg I, Huland DM, Vermesh O, Frostig HE, Tummers WS, Gambhir SS. Photoacoustic clinical imaging. *Photoacoustics*. 2019;14:77–98.
[2] Upputuri PK, Pramanik M. Recent advances in photoacoustic contrast agents for in vivo imaging. *WIRESNanomed Nanobiotechnol*. 2020;12, e1618.
[3] Oh JT, Li ML, Zhang HF, Maslov K, Stoica G, Wang LV. Three-dimensional imaging of skin melanoma in vivo by dual-wavelength photoacoustic microscopy. *J Biomed Opt*. 2006;11, 034032.
[4] Yang S, Tan X, Tang L, Yang Q. Near-Infrared-II bioimaging for in vivo quantitative analysis. *Front Chem*. 2021;9, 763495.
[5] He C, Zhu J, Zhang H, Qiao R, Zhang R. Photoacoustic imaging probes for theranostic applications. *Biosensors*. 2022;12, 947.
[6] Li J, Rao J, Pu K. Recent progress on semiconducting polymer nanoparticles for molecular imaging and cancer phototherapy. *Biomaterials*. 2018;155:217–235.
[7] Wang Y, Feng L, Wang S. Conjugated polymer nanoparticles for imaging, cell activity regulation, and therapy. *Adv Mater*. 2019;29, 1806818.
[8] MacFarlane LR, Shaikh H, Garcia-Hernandez JD, Vespa M, Fukui T, Manners I. Functional nanoparticles through pi-conjugated polymer self-assembly. *Nat Rev Mater*. 2021;6:7–26.
[9] Sanoj Rejinold N, Choi G, Choy J-H. Recent developments on semiconducting polymer nanoparticles as smart photo-therapeutic agents for cancer treatments – a review. *Polymers*. 2021;13, 981.
[10] Kasai H, Nalwa HS, Oikawa H, et al. A novel preparation method of organic microcrystals. *Jpn J Appl Phys*. 1992;31:1132–1134.
[11] Landfester K. The generation of nanoparticles in miniemulsions. *Adv Mater*. 2001;13:765–768.
[12] Tritschler U, Pearce S, Gwyther J, Whittell GR, Manners I. 50th Anniversary perspective: functional nanoparticles from the solution self-assembly of block copolymers. *Macromolecules*. 2017;50:3439–3463.
[13] Valencia PM, Farokhzad OC, Karnik R, Langer R. Microfluidic technologies for accelerating the clinical translation of nanoparticles. *Nat Nanotechnol*. 2012;7:623–629.
[14] Wang Z, Guo B, Middha E, et al. Microfluidics-prepared uniform conjugated polymer nanoparticles for photo-triggered immune microenvironment modulation and cancer therapy. *ACS Appl Mater Interfaces*. 2019;11:11167–11176.
[15] Blanco E, Shen H, Ferrari M. Principles of nanoparticle design for overcoming biological barriers to drug delivery. *Nat Biotechnol*. 2015;33:941–951.
[16] Howes P, Green M, Levitt J, Suhling K, Hughes M. Phospholipid encapsulated semiconducting polymer nanoparticles: their use in cell imaging and protein attachment. *J Am Chem Soc*. 2010;132:3989–3996.
[17] Pu K, Shuhendler AJ, Jokerst JV, et al. Semiconducting polymer nanoparticles as photoacoustic molecular imaging probes in living mice. *Nat Nanotechnol*. 2014;9:233–239.
[18] Jiang Y, Upputuri PK, Xie C, et al. Metabolizable semiconducting polymer nanoparticles for second near-infrared photoacoustic imaging. *Adv Mater*. 2019;31, 1808166.
[19] Stahl T, Bofinger R, Lam I, et al. Tunable semiconducting polymer nanoparticles with INDT-based conjugated polymers for photoacoustic molecular imaging. *Bioconj Chem*. 2017;28:1734–1740.
[20] Nichols JW, Bae YH. EPR: evidence and fallacy. *J Controlled Release*. 2014;190:451–464.
[21] Danhier F. To exploit the tumor microenvironment: since the EPR effect fails in the clinic, what is the future of nanomedicine? *J Control Release*. 2016;244:108–121.
[22] Natfij AA, Ravishankar D, Osborn HMI, Greco F. Parameters affecting the enhanced permeability and retention effect: the need for patient selection. *J Pharm Sci*. 2017;106:3179–3187.

[23] Shi Y, van der Meel R, Chen X, Lammers T. The EPR effect and beyond: strategies to improve tumor targeting and cancer nanomedicine treatment efficacy. *Theranostics*. 2020;10:7921–7924.
[24] Fan Q, Cheng K, Yang Z, et al. Perylene-diimide-based nanoparticles as highly efficient photoacoustic agents for deep brain tumor imaging in living mice. *Adv Mater*. 2015;27:843–847.
[25] Li YQ, Liu J, Liu B, Tomczak N. Highly emissive PEG-encapsulated conjugated polymer nanoparticles. *Nanoscale*. 2012;4:5694–5702.
[26] Wu J, Lee HJ, You L, et al. Functionalized NIR-II semiconducting polymer nanoparticles for single-cell to whole-organ imaging of PSMA-positive prostate cancer. *Small*. 2020;16, 2001215.
[27] Li J, Zhen X, Lyu Y, Jiang Y, Huang J, Pu K. Cell membrane coated semiconducting polymer nanoparticles for enhanced multimodal cancer phototheranostics. *ACS Nano*. 2018;12:8520–8530.
[28] Qiu T, Lan Y, Wei Z, et al. In vivo multi-scale photoacoustic imaging guided photothermal therapy of cervical cancer based on customized laser system and targeted nanoparticles. *Int J Nanomed*. 2021;16:2879–2896.
[29] Cui C, Yang Z, Hu X, et al. Organic semiconducting nanoparticles as efficient photoacoustic agents for lightening early thrombus and monitoring thrombolysis in living mice. *ACS Nano*. 2017;11:3298–3310.
[30] Grandis JR, Sok JC. Signaling through the epidermal growth factor receptor during the development of malignancy. *Pharmacol Ther*. 2004;102:37–46.
[31] Sasaki T, Hiroki K, Yamashita Y. The role of epidermal growth factor receptor in cancer metastasis and microenvironment. *Biomed Res Int*. 2013, 546318.
[32] Master AM, Sen GA. EGF receptor-targeted nanocarriers for enhanced cancer treatment. *Nanomedicine*. 2012;7:1895–1906.
[33] Cai WQ, Zeng LS, Wang LF, et al. The latest battles between EGFR monoclonal antibodies and resistant tumor cells. *Front Oncol*. 2020;10, 1249.
[34] Li Z, Zhao R, Wu X, et al. Identification and characterization of a novel peptide ligand of epidermal growth factor receptor for targeted delivery of therapeutics. *FASEB J*. 2005;19:1978–1985.
[35] Genta I, Chiesa E, Colzani B, Modena T, Conti B, Dorati R. GE11 peptide as an active targeting agent in antitumor therapy: a minireview. *Pharmaceutics*. 2018;10:2.
[36] Song S, Liu D, Peng J, et al. Novel peptide ligand directs liposomes toward EGF-R high-expressing cancer cells *in vitro* and *in vivo*. *FASEB J*. 2009;23:1396–1404.
[37] Han CY, Yue LL, Tai LY, et al. A novel small peptide as an epidermal growth factor receptor targeting ligand for nanodelivery in vitro. *Int J Nanomed*. 2013;8:1541–1549.
[38] Bofinger R, Zaw-Thin M, Mitchell NJ, et al. Development of lipopolyplexes for gene delivery: a comparison of the effects of differing modes of targeting peptide display on the structure and transfection activities of lipopolyplexes. *J Pept Sci*. 2018;24, e3131.
[39] Weitsman G, Mitchell NJ, Evans R, et al. Detecting intratumoral heterogeneity of EGFR activity by liposome-based *in vivo* transfection of a fluorescent biosensor. *Oncogene*. 2017;36:3618–3628.
[40] Bofinger R, Weitsman G, Evans R, et al. Drug delivery, biodistribution and anti-EGFR activity: theragnostic nanoparticles for simultaneous *in vivo* delivery of tyrosine kinase inhibitors and kinase activity biosensors. *Nanoscale*. 2021;13:18520–18535.
[41] Almeida BO, Nag OK, Rogers KE, Delhanty JB. Recent progress in bioconjugation strategies for liposome-mediated drug delivery. *Molecules*. 2020;25, 5672.
[42] Ravasco JMJM, Faustino H, Trinidade A, Gois PMP. Bioconjugation with maleimides: a useful tool for chemical biology. *Chem – Eur J*. 2019;25:43–59.
[43] Zhu H, Fang Y, Zhen X, et al. Multilayered semiconducting polymer nanoparticles with enhanced NIR fluorescence for molecular imaging in cells, zebrafish and mice. *Chem Sci*. 2016;7:5118–5125.
[44] Qin X, Chen H, Yang H, et al. Photoacoustic imaging of embryonic stem cell-derived cardiomyocytes in living hearts with ultrasensitive semiconducting polymer nanoparticles. *Adv Funct Mater*. 2018;28, 1704939.
[45] Pecher J, Mecking S. Nanoparticles of conjugated polymers. *Chem Rev*. 2010;110:6260–6279.
[46] Kurokawa N, Yoshikawa H, Hirota N, Hyodo K, Masuhara H. Size-dependent spectroscopic properties and thermochromic behavior in poly(substituted thiophene) nanoparticles. *ChemPhysChem*. 2004;5:1609–1615.
[47] Wu C, Szymanski C, McNeill J. Preparation and encapsulation of highly fluorescent conjugated polymer nanoparticles. *Langmuir*. 2006;22:2956–2960.
[48] Gandham SK, Talekar M, Singh A, Amiji MM. Inhibition of hexokinase-2 with targeted liposomal 3-bromopyruvate in an ovarian tumor spheroid model of aerobic glycolysis. *Int J Nanomed*. 2015;10:4405–4423.
[49] Rundlöf T, Mathiasson M, Bekiroglu S, Hakkarainen B, Bowden T, Arvidsson T. Survey and qualification of internal standards for quantification by $^{1}$H NMR spectroscopy. *J Pharm Biomed Anal*. 2010;52:645–651.
[50] Li T, Takeoka S. Enhanced cellular uptake of maleimide-modified liposomes via thiol-mediated transport. *Int J Nanomed*. 2014;9:2849–2861.
[51] Du C, Qi Y, Zhang Y, et al. Epidermal growth factor receptor-targeting peptide nanoparticles simultaneously deliver gemcitabine and Olaparib to treat pancreatic cancer with *Breast Cancer 2 (BRCA2)* mutation. *ACS Nano*. 2018;12:10785–10796.
[52] Zhao N, Williams TM, Zhou Z, et al. Synthesis of BODIPY-peptide conjugates for fluorescence labeling of EGFR overexpressing cells. *Bioconj Chem*. 2017;28:1566–1579.
[53] Ringhieri P, Diaferia C, Galdiero S, Palumbo R, Morelli G, Accardo A. Liposomal doxorubicin doubly functionalized with CCK8 and R8 peptide sequences for selective intracellular drug delivery. *J Pept Sci*. 2015;21:415–425.
[54] Phyo P, Zhao X, Templeton AC, Xu W, Cheung JK, Su Y. Understanding molecular mechanisms of biologics drug delivery and stability from NMR spectroscopy. *Adv Drug Deliv Rev*. 2021;174:1–29.
[55] Garcia-Fuentes M, Torres D, Martin-Pastor M, Alonso MJ. Application of NMR spectroscopy to the characterization of PEG-stabilized lipid nanoparticles. *Langmuir*. 2004;20:8839–8845.
[56] Doyen C, Larquet E, Coureux P-D, et al. Nuclear magnetic resonance spectroscopy: a multifaceted toolbox to probe structure, dynamics, interactions, and real-time *in situ* release kinetics in peptide-liposome formulations. *Mol Pharm*. 2021;18:2521–2539.
[57] Klein K, Loza K, Heggen M, Epple M. An efficient method for covalent surface functionalization of ultrasmall metallic nanoparticles by surface azidation followed by copper-catalyzed azide-alkyne cycloaddition (click chemistry). *ChemNanoMat*. 2021;7:1330–1339.
[58] Ruks T, Loza K, Heggen M, et al. Peptide-conjugated ultrasmall gold nanoparticles (2 nm) for selective protein targeting. *ACS Appl Biomat*. 2021;4:945–965.
[59] Goddard ZR, Beekman AM, Cominetti MMD, et al. Peptide directed phthalocyanine-gold nanoparticles for selective photodynamic therapy of EGFR overexpressing cancers. *RSC Med Chem*. 2021;12:288–292.
[60] Mayr J, Hager S, Koblmüller B, et al. EGFR-targeted peptide-coupled platinum(IV) complexes. *J Biol Inorg Chem*. 2017;22:591–603.
[61] Xu Y, Fourniols T, Labrak Y, Préat V, Beloqui A, des Rieux A. Surface modification of lipid-based nanoparticles. *ACS Nano*. 2022;16:7168–7196.
[62] Biscaglia F, Ripani G, Rajendran S, et al. Gold nanoparticle aggregates functionalized with cyclic RGD peptides for targeting and imaging of colorectal cancer cells. *ACS Appl Nano Mater*. 2019;2:6436–6444.